

Improving Sensitivity and Source Attribution of Homemade Explosives with Low Frequency/THz-Raman[®] Spectroscopy

James T.A. Carriere, Frank Havermeier, Randy A. Heyler
Ondax Inc., 850 E. Duarte Rd., Monrovia, CA, USA, 91016

ABSTRACT

Rapid identification and source attribution of homemade explosives (HMEs) is vital to national defense and homeland security efforts. Since HMEs can be prepared in a variety of methods with different component ingredients, telltale traces can be left behind in the final structural form of the material. These differences manifest as polymorphs, isomers, conformers or even contaminants that can all impact the low energy vibrational modes of the molecule. Conventional Raman spectroscopy systems confine their measurements to the “chemical fingerprint” region and are unable to detect low frequency Raman signals ($<200\text{cm}^{-1}$) where these low energy modes are found. This gap in sensitivity limits the conclusions that can be drawn from a single Raman measurement and creates the need for multiple measurement techniques to confirm any results.

We present results from a new rugged, portable approach that is capable of extending the range of Raman to include these low frequency signals down to $\sim 5\text{cm}^{-1}$, plus complementary anti-Stokes spectra, with measurement times on the order of seconds. We demonstrate the diversity of signals that lie in this region that directly correlate to the molecular structure of the material, resulting in a new Raman “structural fingerprint” region. By correlating the measured results with known samples from a spectral library, rapid identification of the specific method of manufacture can be made.

Armed with this additional information about the methods and materials used to manufacture HMEs, officials can use this approach to rapidly respond to threats.

Keywords: Low-frequency Raman, THz-Raman, Homemade explosives, Polymorphs, Isomers, Conformers, Methods of manufacture, Source attribution.

1. INTRODUCTION

Raman spectroscopy is widely incorporated as a means of material identification by detecting the chemical composition of a material via its “fingerprint” of vibrational energies. The fingerprint region corresponds to vibrational modes of the various functional groups of the molecule that are found from about 200cm^{-1} to $>2,000\text{cm}^{-1}$ while lower energy modes ($<200\text{cm}^{-1}$) correspond to vibrational modes of the entire molecular structure or crystal lattice of the material under test¹. This low frequency region (Figure 1) is also referred to as the THz-Raman[®] region because it corresponds to Raman scattering interactions with energy levels in the terahertz range ($5\text{cm}^{-1} - 200\text{cm}^{-1} = 150\text{ GHz} - 6\text{ THz}$) of absorption spectroscopy. Structural vibrations of the molecule can be much more sensitive to changes in the specific molecular formulation because the presence of nearby atoms, functional groups or other molecular co-solvents/co-crystals and contaminants will perturb the structural form of the molecule, and change the required excitation energy of these low frequency modes. Examples of structural differences that have been reported as readily detectable by low frequency/THz-Raman[®] spectroscopy include polymorphs, allotropes and isomers or changes in atomic isotopes²⁻⁸.

The low frequency region is ideal for differentiating subtle changes in HME materials due to different methods of manufacture. With a single measurement, the combined information about both the chemical and structural form of the molecule can be obtained, enabling rapid identification of the chemical composition of the material in addition to information about the pre-cursor ingredients and/or method of manufacture that was used to produce it. Typically several different measurements with various other technologies such as LC/MS, GC/MS, XRD, IR and terahertz absorption would be required in conjunction with Raman to completely characterize the material. This is quite costly and can take hours or even days to get actionable information about the material.

overall throughput of the already weak Raman signal, and (4) still does not provide simultaneous access to both Stokes and anti-Stokes signals.

Recent advances in volume holographic grating (VHG) filter technology^{9,10} have enabled the manufacture of exceptionally narrow bandwidth notch filters with very high throughput. Each VHG filter has a notch profile that is designed to diffract *only* the laser wavelength and transmit all others. The ultra-narrow transition bandwidth of these filters enables extremely high attenuation of the laser wavelength (>OD 4 for each filter), while maintaining very high transmission of nearby Raman signals beyond $\sim 5\text{cm}^{-1}$ (Figure 2).

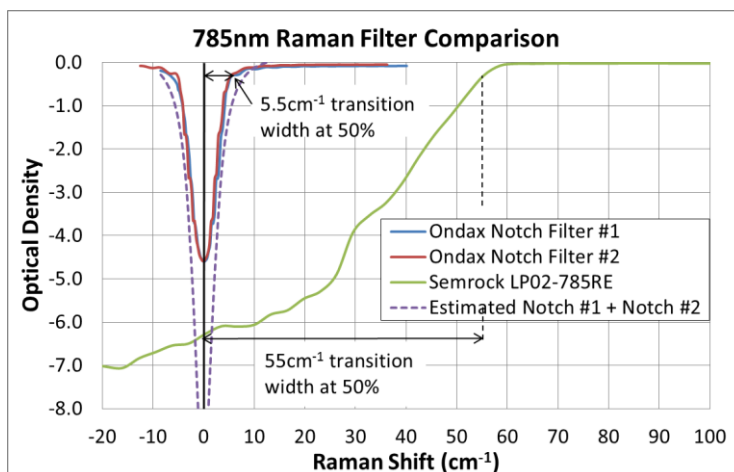


Figure 2. A VHG notch filter has an approximately 10x narrower transition width than a thin-film edge filter, enabling very high Rayleigh attenuation without blocking low-frequency or anti-Stokes Raman signals.

This has led to systems that are capable of rapid acquisition of high-quality, ultra-low frequency Raman spectra in the 5-200 cm^{-1} region. These systems are based on a stable wavelength laser source, a series of VHG filters and a single stage spectrograph (Figure 3). This combination of strong Rayleigh attenuation and high broadband transmission enable the

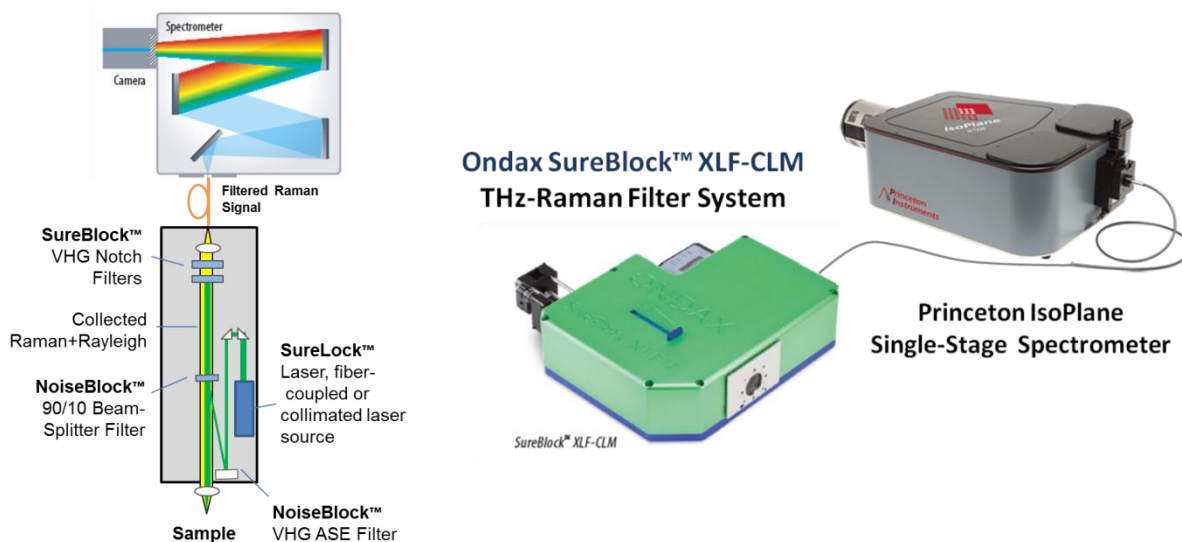


Figure 3. A THz-Raman[®] system is comprised of a compact, confocal optical system that includes a single-frequency/wavelength stabilized laser source, ASE filters, a high-throughput beamsplitter, sample collection optics, and multiple cascaded VHG notch filters. The filtered Raman signal is fed into a single-stage spectrometer for readout. (A schematic of the system is depicted on the left, and a photograph of system used is to the right).

system to simultaneously capture both the intense low-frequency Stokes and anti-Stokes Raman bands and the “fingerprint region” transitions, greatly simplifying the overall system and reducing size and cost, while improving the sensitivity and reliability of using Raman for chemical identification and other applications.

Experimental measurements were taken with the confocal THz-Raman[®] system shown in Figure 3. The system was comprised of a single mode 785nm wavelength stabilized diode laser (SureLock™ LM series, Ondax, Inc.) and a series of ultra-narrowband VHG filters that were spectrally matched to the laser output wavelength. Two VHG ASE suppression filters (NoiseBlock™, Ondax, Inc.) were used to remove amplified spontaneous emission (ASE) from the laser. (ASE is often on the same order of magnitude or larger than the Raman signals, which can reduce SNR or swamp low frequency signals if it is not attenuated). A dichroic 90/10 VHG beamsplitter filter (NoiseBlock™, Ondax, Inc.) redirects the laser towards the sample, where a10X objective lens focuses the laser onto the sample and collects the back-scattered light. The 90/10 beamsplitter then reflects 90% of the Rayleigh scatter back towards the laser while transmitting all of the Raman shifted signals. (The dichroic nature of the 90/10 beamsplitter results in an almost 4X improvement in collected Raman signal compared to a broadband 50/50 beamsplitter). Two ultra-narrowband VHG notch filters (SureBlock™, Ondax, Inc.), each having optical density >4.0, then further attenuate the collected Rayleigh scattered light while transmitting the Raman signals with an estimated system transmission efficiency of >80%. The filtered signal was focused into a 25µm core diameter, 0.1NA step index fiber (HPSC25, ThorLabs) and connected to a high-resolution, high-throughput single stage 0.3m imaging spectrometer (IsoPlane series, Princeton Instruments). It was equipped with a 1200 lines/mm grating and a 1340x400 imaging array (Pixis model 400BR with eXcelon, Princeton Instruments) with 20 x 20 µm pixel size and 98% peak quantum efficiency to ensure maximum signal collection and ~1.25cm⁻¹ resolution; appropriately matched for analysis of the 5-200cm⁻¹ frequency range. (Note: the range, resolution, and noise level of the overall system is ultimately determined by the specifications of the spectrometer, including grating, detector, and size).

The entire laser and filter assembly is extremely compact – approximately the size of a ream of notebook paper – and the fiber coupling allows for remote location of the spectrometer. The low power requirements of the laser also enable the filter system to be battery operated. Finally, it is important to note that the ultra-narrow bandwidth of the VHG filters (<0.1nm) require the use of either a wavelength-stabilized diode laser, narrow-band DPSS laser, or gas laser. Normal diode lasers tend to mode hop, shifting the laser wavelength outside the blocking range of the filters and resulting in either reduced Rayleigh suppression or a complete loss of signal in the described configuration.

3. PREPARATION AND MEASUREMENT OF HME MATERIALS

Pure samples of the following energetic compounds and pre-cursor materials were prepared for analysis with the system that was outlined in the previous section by the Edgewood Chemical Biological Center (ECBC), a U.S. Army RDECOM laboratory:

- Urea
- Urea Nitrate (UN)
- 2,4,6 trinitrotoluene (TNT)
- RDX
- PETN
- Potassium Chlorate (PC)
- Potassium Nitrate (PN)
- HMX
- Ammonium Nitrate (AN)
- 2,6 dinitrotoluene (DNT)
- 2,4 dinitrotoluene (DNT)

The samples were placed into ½ dram glass vials for measurement by the system. Measurements for each compound were taken with 10 second integration time and 3 coadds for a total of 30 seconds.

To test different synthetic pathways, 16 different ETN samples were prepared by Signature Science using different combinations of pre-cursor materials varying from laboratory grade to over the counter. Both mixed acids and strong acids were used for an acid based preparation route while various nitrate salts were used for the salt nitration preparation route. The matrix of sample preparations used for the synthetic pathway analysis is show in Figure 4.

ETN Prep & Analysis #	Erythritol Source	Nitric Acid	Surfuric Acid	Salt	Prep Route	Temp (°C)	Recrystallized (Y/N)	Appearance
1	Lab grade	Lab grade (70%)	Lab grade (conc)	N/A	Mixed Acids (MA)	< 10	Y	white powder
2	Lab grade	Lab grade (70%)	Lab grade (conc)	N/A	Mixed Acids (MA)	< 10	N	off-white powder
3	Truvia	OTC (70%)	OTC-1	N/A	Mixed Acids (MA)	< 10	N	off-white powder
4	Z Sweet	OTC (70%)	OTC-2	N/A	Mixed Acids (MA)	< 10	N	yellow-brown paste
5	Lab grade	Lab grade (90%)	Lab grade (conc)	N/A	Strong Acids (SA)	< 10	N	white powder
6	Truvia	Lab grade (90%)	OTC-1	N/A	Strong Acids (SA)	< 10	N	off-white powder
7	Truvia	OTC (90%)	Lab grade (conc)	N/A	Strong Acids (SA)	< 10	N	white powder
8	Lab grade	N/A	Lab grade (conc)	Ammonium nitrate (Lab grade)	Salt Nitration (SN)	~20	N	white powder
9	Truvia	N/A	OTC-1	Ammonium nitrate (OTC - fertilizer)	Salt Nitration (SN)	~20	N	off-white powder
10	Lab grade	N/A	Lab grade (conc)	Potassium nitrate (Lab grade)	Salt Nitration (SN)	~20	N	white powder
11	Truvia	N/A	OTC-1	Potassium nitrate (OTC - stump remover)	Salt Nitration (SN)	~20	N	off-white powder
12	Lab grade	N/A	Lab grade (conc)	Strontium nitrate (Lab grade)	Salt Nitration (SN)	~20	N	white powder
13	Truvia	N/A	OTC-1	Strontium nitrate (Lab grade)	Salt Nitration (SN)	~20	N	white powder
14	Lab grade	N/A	Lab grade (conc)	Calcium ammonium nitrate (OTC)	Salt Nitration (SN)	~20	N	light brown powder
15	Truvia	N/A	OTC-1	Calcium ammonium nitrate (OTC)	Salt Nitration (SN)	~20	N	light brown powder
16	Lab grade	Lab grade (90%)	Lab grade (conc)	N/A	Oxley Method	< 10	N	white powder

Figure 4. Matrix of erythritol tetranitrate (ETN) preparation routes used to test the sensitivity of THz-Raman[®] to different synthetic pathways.

In each case, the ETN content was validated by direct infusion ESI-MS. The samples were measured as prepared, without purification by recrystallization to represent results that would typically be found in HMEs. A single batch was prepared for each synthetic pathway and three aliquots were prepared for independent testing. Sample #4 had begun to degrade into a paste by the time measurements were performed so only a single aliquot sample was prepared and analyzed in this case. Photographs of the prepared samples are shown in Figure 5.

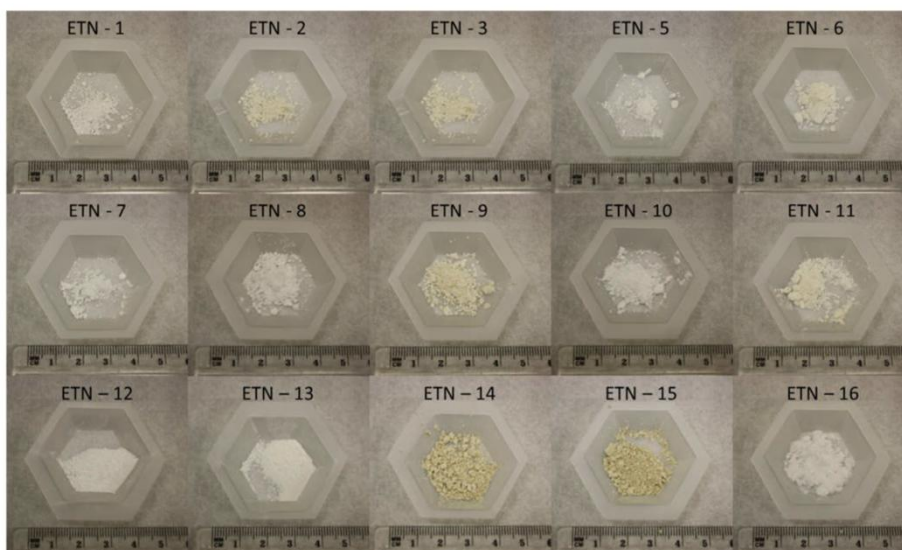


Figure 5. Photographs of ETN samples produced by the methods indicated in Figure 4.

Five additional “blind samples” were taken from the samples with the identity hidden from the tester until after analysis was completed. Once again, all samples were placed into ½ dram glass vials for measurement by the system.

All samples were measured with 10s integration time for each spectral capture region of $\sim 600\text{cm}^{-1}$ with a resolution of $\sim 1.25\text{cm}^{-1}$ and then scanned over 6 steps spanning a total spectral range of -300cm^{-1} to 3000cm^{-1} using the Princeton Instruments step and glue procedure in their LightField software. The total measurement time for each sample was $\sim 60\text{s}$.

The first aliquot samples of each preparation route were actively aligned to maximize the Raman signal and were used as the basis for the spectral library work. The two remaining aliquots for each sample (excluding #4) were then simply placed into the system without active alignment to test the functional discrimination capability of the library.

4. EXPERIMENTAL RESULTS

4.1 Common HME Spectral Analysis

The spectra obtained for the common HME samples are shown in Figure 6. Each sample shows multiple strong peaks in the low wavenumber region of the spectrum when compared with the fingerprint region of the full spectrum. The expanded view of only the low wavenumber region (right side) shows this in greater detail to emphasize the distinct differences between the various samples in such a compact spectral region. Note that in many cases, the low wavenumber signals can be several times larger than the signals in the fingerprint region, indicating a larger Raman scattering cross-section for those vibrational modes. In general, more complex molecular structures tend to exhibit more diverse low wavenumber signals due to increased vibrational degrees of freedom for the molecule while less complex structures exhibit fewer peaks in the entire spectrum.

A cross correlation analysis approach was used to compare the differentiability of the low wavenumber region ($0 - 200\text{cm}^{-1}$) relative to the fingerprint region ($200 - 1678\text{cm}^{-1}$) and the total range ($0 - 1678\text{cm}^{-1}$). Since there was a strong glass background in several of the spectra from the glass vials above $\sim 1300\text{cm}^{-1}$, this signature was corrected using a median iterative filter technique having a width of 20% of the original signal length. The level of dissimilarity was then calculated in each case as $(1 - \text{correlation})$ so that values close to 1 will yield high differentiability and values close to 0 will indicate low differentiability in that region.

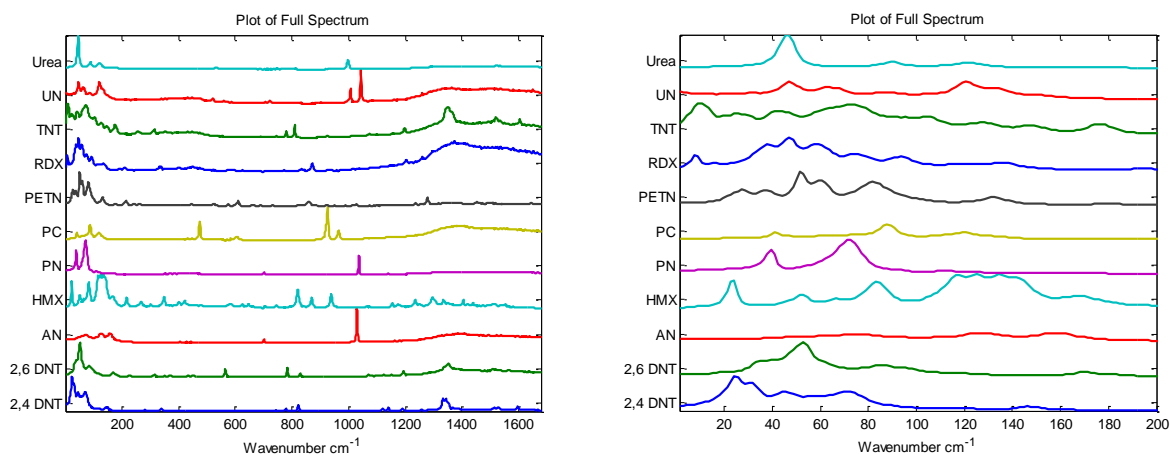


Figure 6. Measured Raman spectra of common HME materials as collected by the system. The left plot shows the full measured range from $0 - 1678\text{cm}^{-1}$ while the right plot shows more detail on the low frequency (low wavenumber) region from $0 - 200\text{cm}^{-1}$.

First, to quantify the ability to discriminate between different isomers the DNT samples were compared against each other and against TNT (Figure 7). While the degree of differentiability isn't particularly high for any case, the low wavenumber region shows the largest distinction with values between 0.5 and 0.6, compared to 0.25 to 0.33 for the fingerprint region alone, and slightly higher (~ 0.35) for the full spectrum results. This is likely due to the fact that isomers are chemically very similar to each other (i.e. very little impact on the chemical fingerprint region), but the significant structural change (of the location on the toluene ring structure of the nitro group) affects the low-frequency vibrational modes of the entire molecule, as clearly manifested in the $<200\text{cm}^{-1}$ region.

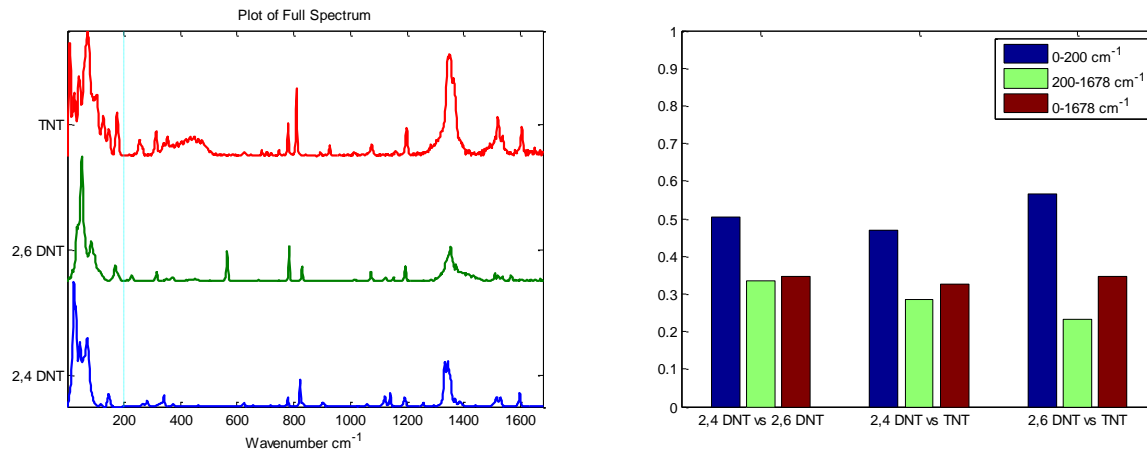


Figure 7. Comparison of the degree of dissimilarity for different DNT and TNT isomers showing analysis results of the low frequency (low wavenumber) region, chemical fingerprint region and full spectrum.

Similar analysis was performed for the inorganic nitrate salts that were measured (Figure 8). This time there is a very high degree of differentiability in almost all cases. When comparing AN vs. PN, the low wavenumber region and the chemical fingerprint region are almost identical in their ability to effectively discriminate between the two materials. But comparing AN vs. UN, the strong extra peak in the fingerprint region of UN makes it highly differentiable while the low wavenumber region peaks are more similar thus reducing the differentiability both there and in the full spectrum. Conversely, when comparing AN vs. PN, the signals in the fingerprint region are somewhat similar but those in the low wavenumber region are very different and giving them a clear advantage for discriminating between the two materials.

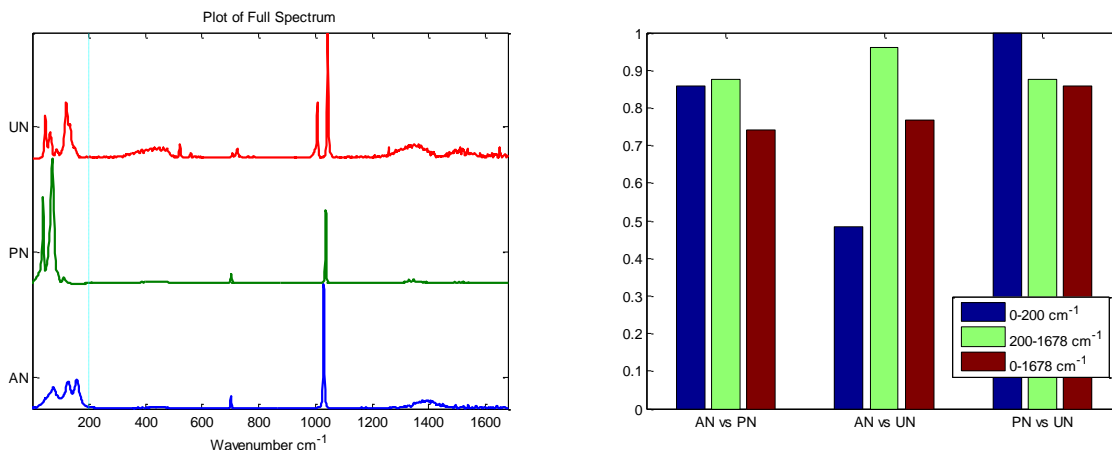


Figure 8. Comparison of the degree of dissimilarity for different inorganic nitrate salts showing analysis results of the low wavenumber region, chemical fingerprint region and full spectrum.

4.2 ETN Spectral Library Construction

Spectra were obtained (from -300cm^{-1} to $>3,000\text{cm}^{-1}$) on all 16 ETN samples. Ten of the sixteen samples exhibited minimal fluorescence and are shown in Figures 9 and 10. (All other fluorescent spectra were still included in the spectral library and used for comparison with the blind sample measurements). The large, broad hump in the signals between 1300cm^{-1} and 2000cm^{-1} was due to the glass vials that were used to contain the samples in the system. Since there appear to be no significant signals in this region that relate to the ETN material itself, the spectral analysis was confined to regions below this region from -300cm^{-1} to 1300cm^{-1} .

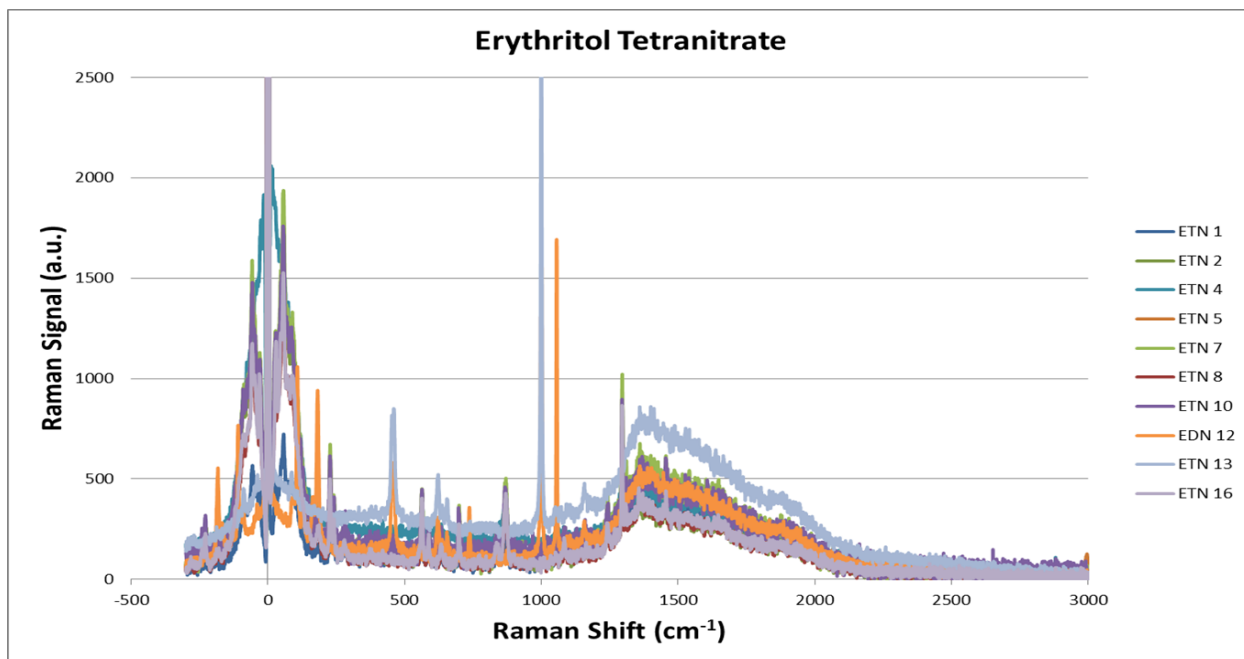


Figure 9. THz-Raman[®] spectral measurements of ETN showing both the low wavenumber and chemical fingerprint regions for the samples that did not exhibit strong fluorescence.

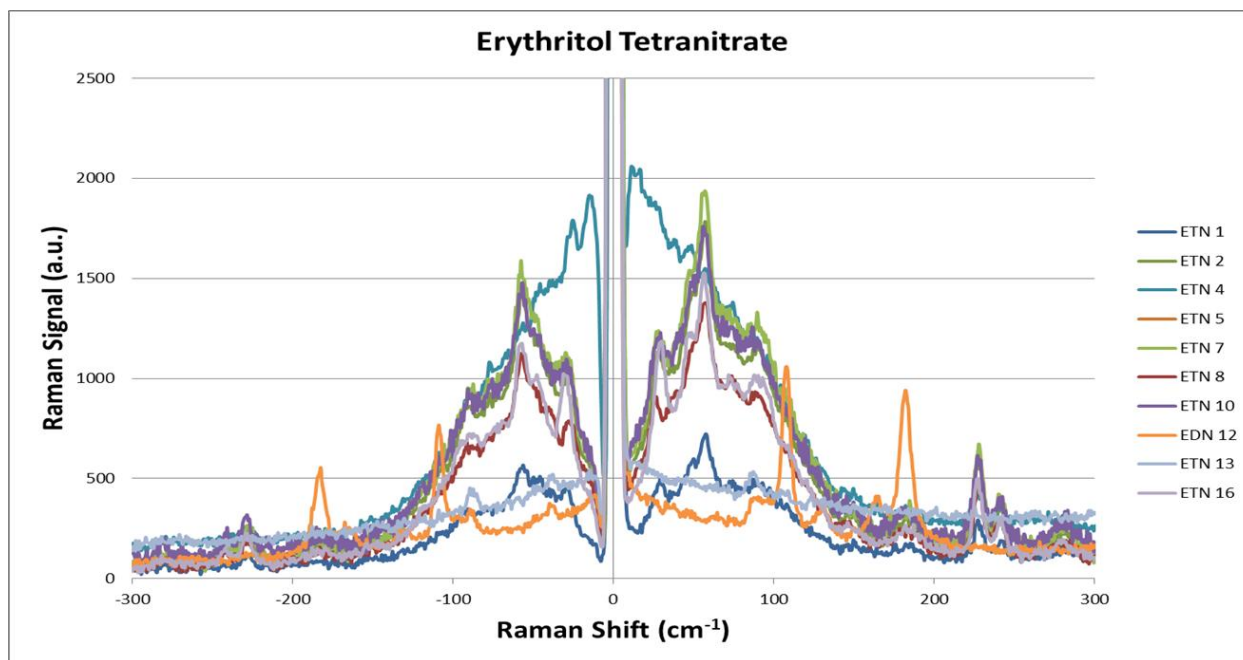


Figure 10. Expanded view of the low frequency Stokes+anti-Stokes THz-Raman[®] region for the ETN samples that did not exhibit strong fluorescence.

The carefully aligned spectral data from the first aliquot from each sample was used to create a spectral library with a commercially available software program called Panorama by LabCognition. Follow-on spectral data from the remaining two aliquots that were simply placed in the system and not optimized for maximum Raman signal were used to determine the threshold for sample identification. Each of the secondary and tertiary aliquot sample spectra were compared to the full spectral library from the first aliquot samples by using the simple scalar product matching function

from the software. The region around the Rayleigh line ($\pm 8\text{cm}^{-1}$) was removed from the library analysis to prevent the software from providing false readings based on signals that were not related to the Raman scattering modes of the sample.

The resulting fit ratio values determined by the scalar product algorithm were tabulated and compared for each sample. An average and standard deviation for a correct “hit” was determined by analyzing the resultant fit ratio value for the correct sample in all cases. By this method, the average “correct” fit ratio was 98.05 and the standard deviation was 2.40. This indicates that any corresponding spectral fit ratios to the library for unknown samples would be deemed statistically significant when larger than 95.65 and likely candidates when larger than 98.05.

4.3 ETN Blind Sample Analysis

Once the library was created and the corresponding values for statistical significance were obtained, the blind samples were compared with the full spectral library using the same scalar product algorithm. Figure 11 shows the corresponding fit ratios that were obtained for each of the five blind samples. The highlighted sections represent the potential candidates that had fit ratios of >98.05 . This indicates that the original sample set of 16 candidates could be immediately reduced to between 2 and 6 likely candidates.

ETN Sample	Blind Sample A	Blind Sample B	Blind Sample C	Blind Sample D	Blind Sample E
1	95.95	97.5	74.25	93.99	76.63
2	99.83	99.71	69.29	94.16	68.51
3	66.13	67.32	99.93	87.7	98.12
4	92.46	91.56	63.31	86.29	62.35
5	99.63	99.82	68.75	93.83	68.57
6	91.5	92.19	90.66	99.63	89
7	99.29	99.68	70.78	94.45	70.98
8	99.63	99.69	69.48	94.06	69.15
9	74.45	75.58	99.43	92.76	97.88
10	99.1	99.45	72.85	95.26	73.03
11	96.98	97.03	82.51	98.98	80.34
12	64.53	65.96	70.13	71.86	73.23
13	68.72	70.52	70.22	74.06	74.05
14	76.08	77.26	99.12	93.63	97.86
15	65.85	67.39	99.85	87.37	98.93
16	99.5	99.74	69.97	94.25	69.84
# of potential candidates	6	6	4	2	2

Figure 11. Fit ratios of each blind sample compared to the 16 different library components using the simple scalar product method to compare the blind sample spectra with the spectral library. The circled values indicate the actual identity of the blind samples: all except one also had the highest fit ratios.

After this preliminary analysis, the correct identities of the blind samples were revealed to the analyzer, as A = ETN 2, B = ETN 5, C = ETN 9, D = ETN 6, E = ETN 15 corresponding to the circled values in Figure 11. In 4 out of 5 cases (80%), the highest fit ratio result for the blind samples correctly identified the blind ETN sample. With further improvements to the fit model and additional data to improve the spectral library, this accuracy level could be significantly improved.

5. CONCLUSIONS

The low frequency THz-Raman[®] region was demonstrated to have significant information that can be used for material identification and forensic analysis for a number of explosives materials and precursor elements. Depending on the

specific material that is being measured, the spectral data obtained from the low wavenumber “structural fingerprint” region can be similar or significantly more differentiating than the chemical fingerprint region. Using a simple spectral library and non-specific analysis routine, a single rapid measurement of a blind ETN sample on the order of seconds can be used to down-select the number of statistically significant potential synthetic pathways by a factor of 2.6-8 and accurately identify the unknown material 80% of the time. The accuracy of the library could be further improved by adding additional sample aliquots and multiple different batches to the analysis to reduce the standard deviation. Improvements to the algorithm could also be made for ETN specifically by restricting the analysis region to specific known peaks for ETN and using a dedicated PCA-PLS algorithm. With further developmental work, this system can be easily miniaturized into a portable solution that can be taken into the field and is able to deliver potentially actionable information about the origin of the HME under test.

ACKNOWLEDGMENTS

We gratefully acknowledge the contributions of Jason Guicheteau, Darren Emge and Augustus Way Fountain of the Edgewood Chemical Biological Center, a U.S. Army RDECOM Laboratory for their measurement and analysis of the common explosives and inorganic nitrate salts. We would also like to acknowledge Joe Chipuk and Amanda Meyer of Signature Science for their work in preparing the ETN samples for analysis. Finally, we would like to thank Princeton Instruments for providing the spectrometer and their ongoing support of our application development work.

REFERENCES

- [1] Larkin, P. J., Dabros, M., Sarsfield, B., Chan, E., Carriere, J. T., and Smith, B. C., “Polymorph characterization of active pharmaceutical ingredients (APIs) using low-frequency Raman spectroscopy,” *Applied Spectroscopy* 68(07), (2014).
- [2] Hédoux, A., Paccou, L., Guinet, Y., Willart, J.-F., and Descamps, M., “Using the low-frequency Raman spectroscopy to analyze the crystallization of amorphous Indomethacin,” *European Journal of Pharmaceutical Sciences* 38, 156–164 (2009).
- [3] Hédoux, A., Guinet, Y., and Descamps, M., “The contribution of Raman spectroscopy to the analysis of phase transformations in pharmaceutical compounds,” *International Journal of Pharmaceutics* 417 17– 31(2011).
- [4] Carriere, J. T. A., Havermeyer, F., and Heyler, R. A., “THz-Raman spectroscopy for explosives, chemical and biological detection,” *Proc. SPIE* 8710, 87100M (2013).
- [5] Day, G. M., Zeitler, J. A., Jones, W., Rades, T., and Taday, P.F., “Understanding the Influence of Polymorphism on Phonon Spectra: Lattice Dynamics Calculations and Terahertz Spectroscopy of Carbamazepine,” *J. Phys. Chem. B*, 110, 447-456 (2006).
- [6] Oxley, J., Smith, J., Brady, J., Dubnikova, F., Kosloff, R., Zeiri, L., and Zeiri, Y., “Raman and infrared fingerprint spectroscopy of Peroxide-based explosives,” *Applied Spectroscopy* 62(8), 906-915 (2008).
- [7] Wu, H. B., Chan, M. N., and Chan, C. K., “FTIR Characterization of Polymorphic Transformation of Ammonium Nitrate,” *Aerosol Science and Technology*, 41(6), 581-588 (2007).
- [8] Keller, W. E., and Halford, R. S., “Motions of Molecules in Condensed Systems. IV. The Infra-Red Spectra for Ammonium Nitrate and Thallous Nitrate,” *The Journal of Chemical Physics*, 17(1), 26-30 (2004).
- [9] Moser, C. and Havermeyer, F., “Ultra-narrow band tunable laserline notch filter,” *Applied Physics B: Lasers and Optics* 95(3), 597-601 (2009).
- [10] Moser, C. and Havermeyer, F., “Compact Raman spectrometer system for low frequency spectroscopy,” *Proc. SPIE* 7598, 75980S (2010).